IEEE Access
Multidisciplinary | Rapid Review | Open Access Journal

Received November 28, 2019, accepted January 19, 2020, date of publication January 22, 2020, date of current version January 29, 2020.

Digital Object Identifier 10.1109/ACCESS.2020.2968739

Bio-Inspired Tendon-Driven Finger Design With Isomorphic Ligamentous Joint

GEON LEE[1] AND YOUNGJIN CHOI[2], (Senior Member, IEEE)
[1]Department of Electronic System Engineering, Hanyang University, Ansan 15588, South Korea
[2]Department of Electrical and Electronic Engineering, Hanyang University, Ansan 15588, South Korea

Corresponding author: Youngjin Choi (cyj@hanyang.ac.kr)

This work was supported in part by the Convergence Technology Development Program for Bionic Arm of the National Research Foundation of Korea funded by the Ministry of Science, ICT & Future Planning under Grant 2015M3CB2052811, and in part by the National Research Foundation of Korea Grant funded by the Korea Government (MSIT), South Korea, under Grant 2019R1A2C1088375.

ABSTRACT This paper suggests a novel type of bio-inspired finger design in that the joints that compose the finger mimic the features of human finger joints. They have isomorphic structures but different movements, further, there is no friction between bones in the joint, and the joint has a compliance property in all the directions thanks to the elasticity of ligaments. In the proposed joints, a number of strings substitute the articular capsule and collateral ligaments based on the concept of a tensegrity structure. Ultimately, a compliant robotic finger based on the ligamentous structure of the human is proposed. In addition, adjusting the fixed positions of the strings without any structural change, the joint can have a rest position yielded from the elasticity of the strings, and thereby, the tendon is only needed to drive the finger. Especially, since the finger does not have any mechanical rotating parts such as bearings and bushes, it can freely operate even underwater. As the proposed finger design is a type of underactuated mechanism, it is able to realize active flexion, passive extension, and passive adduction and abduction.

INDEX TERMS Biomimetic joints, compliant joints, robotic finger, tendon-driven actuator, tensegrity structure, underactuation.

I. INTRODUCTION

Recently, in the field of robotics the research on biomimetics has increasingly received attention. Biomimetic technology is considered as one of the best ways to resolve human-related issues. Many of the researchers have found the solutions to problems which were once considered as the Gordian knot to cut with well-known methods, from the link with nature. For instance, Collins *et al.* developed passive dynamic walker through morphological approach [1]. Koh *et al.* found the solution to robot walking and jumping on water from the structure of water strider [2]. Sreetharan and Wood presented an innovative insect-scale robotic thorax design able to produce asymmetric wing kinematics similar to flies and other two-winged insects [3]. Garcia *et al.* proposed leg mechanism which could generate agile and powerful locomotion, extracting key principles from horse legs [4].

Especially in the area of human-mimetic robotics, there have been lots of attempts that researchers apply advantages of the human body to the robots. Their results have outperformed traditional robots through biological mimicry of the human bodies. Li *et al.* developed soft actuators for eyeball motion, which mimic muscles in eyes of human [5]. Shirafuji *et al.* introduced an anatomical model of human finger to their tendon-driven robotic finger and revealed a few advantages of the human musculoskeletal structure [6]. Ikemoto *et al.* proposed shoulder mechanism including the glenohumeral and scapulothoracic joints and tried to control the joint mechanism with pneumatic artificial muscles [7]. Ananthanarayanan *et al.* fulfilled high-speed running legs inspired by musculoskeletal structures with foam-core prototyping technique [8]. Xu and Todorov realized dexterous hand through mimicking biomechanical structure of human hand such as artificial joint capsules, crocheted ligaments and tendons [9]. Deshpande *et al.* introduced Anatomically Correct Testbed(ACT) hand and showed outstanding ability of grasping arbitrary object in consequence of replicating biomechanical features of the human hand [10]. Most researches mentioned above, however, only focused on the musculoskeletal systems. Thereby, they overlooked functions

The associate editor coordinating the review of this manuscript and approving it for publication was Hui Xie.

of the ligaments which are able to show another enormous features of the human body.

The joints of human body are enclosed with a variety of ligaments. Different from mechanical joints, two or more bones are not stably interlocked but loosely rested on each other in the human joint. This being so, the joint has little intrinsic skeletal stability in itself. Ligaments enclosing the joint play crucial roles that make the joint stable, restrict its excessive movement, endow the joint with compliant property, and prevent the bones from being dislocated [11]–[15]. Furthermore, the articular capsule wrapping around the joint consists of two layers, synovial layer and fibrous layer. The synovial layer containing fluid helps the joints move smoothly with minimum friction, and the fibrous layer keeps the bone from being dislocated with its tensile forces [16]. Although the ligamentous structure in the human body has lots of merits, unfortunately, it is hard to mimic the human joint by using traditional mechanical units.

One of the crucial advantages in the ligamentous structure is to have a compliance inherently due to the ligaments connected between bones as discussed in [17]. This characteristic of compliance is one of the most important factors in the wearable robot fields. The robots which do not have the compliant property are limited in safety and flexibility during interactions between external environments and objects. Especially, the prosthetics, having compliant feature inherently, are considered very meaningful, since the amputee commonly feels extremity pain more than normal person [18]. Kashiri *et al.* studied variable impedance robot arms driven by compliant actuation systems equipped with a clutch mechanism in parallel to the passive compliant transmissin element [19]. Wolf and Hirzinger developed a new type of variable stiffness joint mechanism featuring a dynamic stiffness adjustment and reifying a concept of ball rolling on the curved surface [20]. Yoon *et al.* developed a passive compliant joint using a magneto-rheological damper and a rotary spring [21]. Cestari *et al.* analyzed the locomotion cycle phase and developed the compliant joint having variable stiffness according to swing phase [22]. These resultant mechanisms seem to suit their purpose, but they have two issues such as they did not provide the compliance to all directions and they were not appropriate as small size joints.

The concept of soft robotics has been introduced as an alternative to implementing the compliant mechanism. As the compliant finger using the pneumatic actuator is one of the most popular methods, it enables not only adaptive grasping but also a compliant movement against external forces [23], [24]. However, it is difficult to have a formalized shape during its motion because it is inflatable, in fact, the finger shape is one of the important factors in prosthetics that values aesthetic. Also, it is hard to limit the degree of freedom in certain joints because the criteria of the joints are not clear. In another way, Odhner *et al.* developed the gripper including compliant fingers whose joints made up of flexible beam [25]. In spite of many advantages of this design, however, it is difficult to actuate the finger efficiently without energy loss because of the friction between the driven tendons and phalanges. In other words, it needs a relatively powerful actuator, thereby it becomes difficult to be manufactured in small size and lightweight.

Tensegrity structure consists of two parts which are compressive part called as rigid body and tensile part as elastic string. The configuration of rigid bodies and elastic strings in equilibrium is referred to as tensegrity structure [26]. It is considerably similar to human ligamentous structure in some aspects. First, the tensile parts composed of strings to mimic human ligaments make the structure kinematically stable. Second, there is little friction between rigid bodies since there is no contact between rigid bodies in the tensegrity structure. Thus, it is plausible that bones and ligaments in the ligamentous structure are substituted with rigid bodies and elastic strings in the tensegrity structure, respectively. Actually, G. Scarr has considered the human elbow complex as tensegrity structure [27]. Major advantages of tensegrity structure in mechanics are listed as follows. First, the tensegrity structure could be relatively lightweight because rigid bodies and strings are only used. Also, it could be relatively thinner than other traditional mechanisms because the rigid bodies in tensegrity structure undergo only compressive forces, not bending forces. Second, the rigid bodies have no contact with each other in the tensegrity structure, that is to say, mechanical damage could be reduced due to low frictional effect [28], [29]. Third, the tensegrity structures have the compliant property inherently due to the strings connectivities.

A novel type of finger design based on biomimetic hinge joints is proposed in this paper. A joint structure mounted at the finger is inspired by ligamentous structure of human joints which have the articular capsule and collateral ligaments. The joint structure consist of two rigid bodies and six elastic strings which mimic the bones and soft tissues; rigid bodies substituting for bones, quadrilateral with four strings standing in for the articular capsule, and a pair of strings corresponding to a pair of collateral ligaments. Especially, function of these soft elements is same feature as that of human joint: they make the joint stable, influence on the direction joint moves, and minimize friction between the rigid bodies. In addition, this paper deals with the tendon routing issue inside the robotic finger as well as the analysis and the modified design of ligamentous joint for having rest configuration. Actually the finger uses single driven tendon for joint flexion, and the modified joint allows joint extension by elastic energy stored in the strings. Ultimately, an underactuated mechanism is chosen as one of the design strategies for feasible robotic hands. The underactuation system is defined as the number of actuators is smaller than the motion degrees-of-freedom (DoFs) [30]. To use as few actuators as possible can decrease size and weight of the finger and also it can be low-cost.

II. JOINT STRUCTURE OF THE HUMAN

A finger of the human is usually regarded as having three joints: distal interphalangeal (DIP) joint, proximal interphalangeal (PIP) joint, and metacarpophalangeal (MCP) joint.

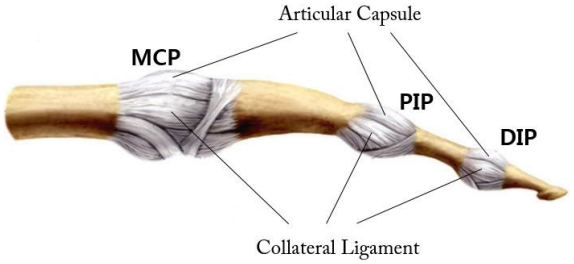

FIGURE 1. Human finger is regarded as having four bones which are metacarpal and three phalanges and three joints which are called MCP, PIP and DIP joints. In detail, the structures of three joints are isomorphic, and each joint is composed of an articular capsule and a pair of collateral ligaments.

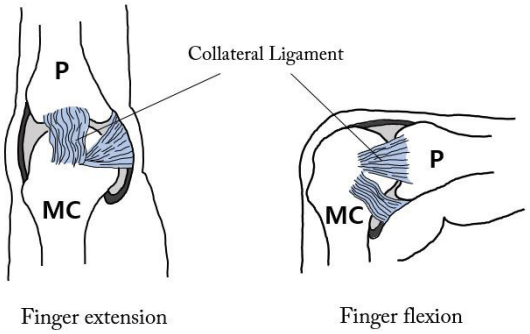

FIGURE 2. In metacarpophalangeal(MCP) joint, the collateral ligaments are attached at dorsal point rather than isometic point. Therefore, the collateral ligaments are loose in metacarpophalangeal joint extension, whereas they are taut in metacapophalangeal joint flexion.

As shown in Figure 1, three joints have a very similar structure including phalanges, articular capsule, and a pair of collateral ligaments—actually there are two types of collateral ligaments which are proper collateral ligaments and accessory collateral ligaments. Indeed, all hinge joints existing our body, for instance, humeroulnar joint in the elbow complex and tibiofemoral joint in the knee, also have similar structure [15]. Although two rigid bodies are sturdily fixed at the same axis in mechanical hinge joints, that is not the case in humans. In the case of human, phalanges are unstably placed end to end. In detail, the distal phalanx simply sits on the pulley-shaped head of a phalanx proximal to it.

These unstable joints become robust and stable by the soft fibrous tissues such as the articular capsule and the ligaments. The articular capsule consists of two layers and plays a primary role as lubrication and stabilizing joint: a fibrous layer attached to the ends of bones keeps the bone from bones from being dislocated each other due to its tensile force; a synovial layer containing a small amount of synovial fluid inside it helps the musculoskeletal structures moving smoothly with minimum friction [16]. The collateral ligaments located on the medial and lateral sides of joints also prevent dislocation of bones. Moreover, the ligaments not only solidify the joint stability against valgus and varus stress, but also restrain excessive medial and lateral movement [12], [14], [15]. Thereby, they are deeply involved in movement of the joint. Furthermore, since the articular capsule and collateral ligaments made up of fiber have flexibility and elasticity themselves, they allow the articular joints to have somewhat of compliance against external force [13], [16].

Although the structures of three joints are isomorphic, they have somewhat different movements. As is well known, PIP and DIP joints are regarded as 1-DoF joint, MCP joint, however, has varying degrees of freedom—usually it is considered 2-DoFs at finger extension and 1-DoF at finger flexion [31]. This is because of dissimilarity in the origins of collateral ligaments which play a role of restraining medial and lateral movements. In detail, the collateral ligaments in the PIP and DIP joint originate isometric point on pulley-shaped head of the proximal phalanx. In other words, the lengths as well as tensile forces of the collateral ligaments remain constant regardless of finger flexion and extension. Whereas these characteristic of collateral ligaments in MCP joint changes with finger flexion and extension. As shown in Figure 2, the collateral ligaments are properly loose at MCP joint extension and taut at the joint flexion. These variations in tensile forces of the ligaments account for the abduction/adduction that can be obtained at the joint in full extension and the minimal amount of abduction/adduction at the joint in full flexion. In addition, this phenomenon is caused by the cam effect attributable to dorsally located collateral ligaments.

To summarize, the ligamentous joint structure has several properties as follows: the joints have isomorphic structure even though having different movements; the joints have somewhat of compliance every direction except rotation direction; the joints have little friction between rigid bodies. These properties of ligamentous structure could not be attained from traditional mechanisms. These properties are also what we want achieve by biomimetics in this paper.

III. LIGAMENTOUS JOINT MECHANISM

A. TWO TYPES OF COMPLIANT JOINT BASED ON TENSEGRITY STRUCTURE

Major advantages of tensegrity structure in mechanics are explained in the following. First, the tensegrity structures are relatively lightweight. Rigid bodies are connected not by mechanical parts, but by strings, and strings are relatively lighter than mechanical components such as mechanical bearing and bush. Moreover, they could be relatively thinner than other traditional mechanism because the rigid bodies in the tensegrity structure do not receive the bending forces, but the compressive forces. Second, there is no contact between the rigid bodies in the tensegrity structure. Every rigid body is seen to be floated in the air because they are in equilibrium by tensile forces. Therefore, the mechanical damage due to friction between rigid bodies could be reduced. Third, the tensegrity structures have somewhat of compliance. While rigid bodies are regarded not to be compliant, strings have flexibility in themselves. As a result, degree of

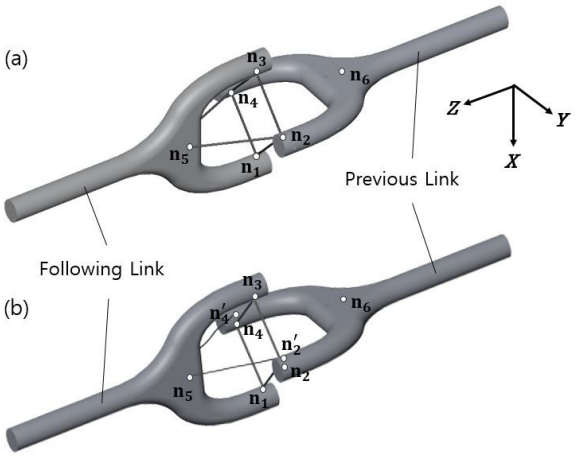

FIGURE 3. Two types of ligamentous joint structure: (a) Type I hinge joint; (b) Type II hinge joint. PIP and DIP joints belong to Type I joint and MCP joint belongs to Type II joint. Two types of joints have isomorphic structure but have different features in their movement.

flexibility in the structure is dependent on elastic modulus of the strings.

Tensegrity structure is similar to ligamentous structure in human body. In the tensegrity structure, elastic strings make the whole structure including rigid bodies stable using their tensile forces. On the other hand, in the human joints, fibrous tissues such as the articular capsule and ligaments deal with the joint stability preventing dislocation of the bones. Ligamentous structure, however, is a little different in arrangement of the strings and in characteristics of the force equilibrium. In the tensegrity structure, strings are usually fixed at the ends of rigid bodies with the same points while ligamentous structures are not. Above all things, tensegrity structure forms stable structure itself in statics. Since the ligamentous structuree does not form stable structure, however, this unstable force equilibrium provides joint characteristics such as axis of rotation, degree of freedom, and so forth.

Two types of hinge joint for constituting finger mechanism are proposed in this section. The one is pure hinge joint such as PIP and DIP joints. Pure hinge joint means mechanically 1-DoF revolute joint which is widely known and used 1-DoF joint, and for the sake of simplicity, this joint is called Type I hinge joint in this paper. Another is alterative hinge joint such as MCP joint. The characteristic of this joint is that its DoFs vary with amount of rotation. In other words, the joint usually has 2-DoFs like universal joint. However, as the joint rotates, range of motion of 1-DoF shrinks to nothing and finally is reduced to just 1-DoF at specific position. Also, for the sake of simplicity, let us call this joint Type II hinge joint. Both types of joints have isomorphic structure, and their mechanisms are made up of two rigid bodies and six elastic strings—actually four main strings and a pair of substrings.

Two types of the proposed joint mechanism are shown in Figure 3. Each string has pretension as tensile force and each rigid body has two branches. The ends of two main strings are joined and fixed at the same point of rigid body branch such as specific points $\mathbf{n}_1$, $\mathbf{n}_2$, $\mathbf{n}_3$, and $\mathbf{n}_4$ as shown in Figure 3. The four main strings form quadrangle shape in a single plane and their tensile forces are maintained in the force equilibrium. Two Substrings originate in the same point on following link and are inserted on different branch of previous link.

Let us consider four main strings without substrings. Since four specific points at which main strings are fixed are no longer move without any external forces, the axes of rotations are found in the diagonal lines connected to two facing points, for example, the rotational axis for roll motion is on the line passing through the points $\mathbf{n}_1$ and $\mathbf{n}_3$, and the rotational axis for pitch motion is on the line from $\mathbf{n}_2$ to $\mathbf{n}_4$. Having two axes of rotations, the mechanism becomes 2 DoFs joint without any external forces. As a matter of fact, the proposed joint mechanism allows three translational motions of X, Y, Z directions as well as the yaw rotational motion as small amounts thanks to the variations of tensile forces of four strings. This phenomenon brings the inherited-compliance to the mechanism, in which the extent of compliance is proportionally dependent on the elasticity of strings.

For the case of Type I joint, adding two substrings obstruct the roll motion of following link because of their tensile forces. As shown in Figure 3(a), fixed locations of a pair of substrings in previous link lie on the line passing through the points $\mathbf{n}_2$ and $\mathbf{n}_4$, namely isometric point. As the lengths of substrings maintain constant regardless of pitch motion, the joint is still able to perform pitch motion freely. Whereas fixed locations of the substrings lie on not isometric points but dorsal points, $\mathbf{n}'_2$ and $\mathbf{n}'_4$, for the case of Type II. Also, substrings are loosely connected as much as they become taut when the following link rotate 90 degrees. As the joint is not influenced by tensile forces of substrings except when it is in full flexion, the joint can perform roll and pitch motions. In joint full flexion, however, roll motion is restricted for the same reason with the Type I case.

B. NODAL ANALYSIS OF THE JOINT STRUCTURE

The ligamentous structure in MCP joint has been modified from those of PIP and DIP joints. Since fixed locations of the substrings on previous link are shifted dorsally for adduction and abduction, all mathematical proofs are based on PIP and DIP joints. In the nodal analysis, the node is defined as a point at which two or more members are joined, and the member is as the smallest unit to express bars and strings. Rigid bodies which are previous and following links having two branches can be represented by three bars. Therefore, the ligamentous joint structure is composed of six nodes and twelve members—six bars and six strings as shown in Figure 4.

The configuration of entire structure is described by a matrix composed of node vectors as follows:

$$\mathbf{N} = \begin{bmatrix} \mathbf{n}_1 & \mathbf{n}_2 & \cdots & \mathbf{n}_6 \end{bmatrix} \in \mathbb{R}^{3\text{x}6}$$

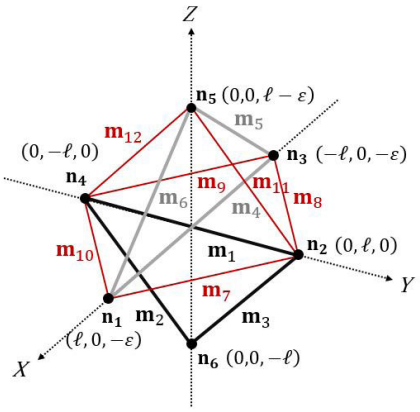

FIGURE 4. Joint structure schematically depicted in 3-dimensional space. two rigid bodies are represented by three bars, which are depicted gray and black lines, respectively. Four main strings and a pair of substrings are depicted by red lines. Note that $\mathbf{n}_1$ and $\mathbf{n}_3$ are located on the XZ-plane, not located on X-axis due to tensil forces in substrings. $\mathbf{n}_2$ and $\mathbf{n}_4$ are located on the YZ-plane and located on Y-axis. $\mathbf{n}_5$ and $\mathbf{n}_6$ are located on Z-axis.

$$= \begin{bmatrix} \ell & 0 & -\ell & 0 & 0 & 0 \\ 0 & \ell & 0 & -\ell & 0 & 0 \\ -\epsilon & 0 & -\epsilon & 0 & \ell-\epsilon & -\ell \end{bmatrix} \tag{1}$$

where $\mathbf{n}_1, \cdots, \mathbf{n}_6 \in \mathbb{R}^3$ are six nodal vectors illustrated in the Figure 4 and $\mathbf{N}$ is a node matrix.

Similarly, the matrix composed of member vectors, member matrix, is defined as:

$$\begin{aligned} \mathbf{M} &= \begin{bmatrix} \mathbf{m}_1 & \mathbf{m}_2 & \cdots & \mathbf{m}_{12} \end{bmatrix} \in \mathbb{R}^{3\text{x}12} \\ &= \begin{bmatrix} 0 & 0 & 0 & -2\ell & \ell & -\ell \\ -2\ell & \ell & -\ell & 0 & 0 & 0 \\ 0 & -\ell & -\ell & 0 & \ell & \ell \\ -\ell & -\ell & \ell & -\ell & 0 & 0 \\ \ell & -\ell & -\ell & -\ell & -\ell & \ell \\ \epsilon & -\epsilon & \epsilon & \epsilon & \ell-\epsilon & \ell-\epsilon \end{bmatrix} \end{aligned} \tag{2}$$

where $\mathbf{m}_k$ denotes the vector that describes the k-th member whose nodes are $\mathbf{n}_{ik}$ and $\mathbf{n}_{jk}$, for example, $\mathbf{m}_1 = \mathbf{n}_4 - \mathbf{n}_2$.

To describe the relationship between members and nodes, the connectivity matrix is introduced. Now define the vector $\mathbf{e}_i \in \mathbb{R}^n$ as the vector with one in the i-th position and zero elsewhere, in which n is the number of nodes. And define the vector $\mathbf{d}_k$ as the member vector in nodal space denoted by $\mathbf{d}_k = \mathbf{e}_{ik} - \mathbf{e}_{jk}$. Then the connectivity matrix is obtained as follows:

$$\begin{aligned} \mathbf{C} &= \begin{bmatrix} \mathbf{d}_1 & \mathbf{d}_2 & \cdots & \mathbf{d}_{12} \end{bmatrix}^T \in \mathbb{R}^{12\text{x}6} \\ &= \begin{bmatrix} 0 & -1 & 0 & 1 & 0 & 0 \\ 0 & 0 & 0 & -1 & 0 & 1 \\ 0 & -1 & 0 & 0 & 0 & 1 \\ -1 & 0 & 1 & 0 & 0 & 0 \\ 0 & 0 & -1 & 0 & 1 & 0 \\ -1 & 0 & 0 & 0 & 1 & 0 \\ -1 & 1 & 0 & 0 & 0 & 0 \\ 0 & -1 & 1 & 0 & 0 & 0 \\ 0 & 0 & -1 & 1 & 0 & 0 \\ -1 & 0 & 0 & 1 & 0 & 0 \end{bmatrix} \end{aligned} \tag{3}$$

The connectivity matrix is made of ones, zeros, and minus ones. In addition, the row vector of this matrix intuitively instructs whose nodes are related with particular member. For instance, the first row vector [0 −1 0 1 0 0] of the connectivity matrix implies that member $\mathbf{m}_1$ is represented by $\mathbf{n}_4 - \mathbf{n}_2$.

The potential energy of the entire structure denoted by V(n) is expressed by a function exclusively of the lengths of members as follows:

$$V(\mathbf{n}) = \sum_{k=1}^{12} V_k(\|\mathbf{m}_k\|) \tag{4}$$

where $V_k(\|\mathbf{m}_k\|)$ denotes the potential energy associated with the k-th member. The total force at the nodes denoted by $\mathbf{f}(\mathbf{n})$ is obtained from derivative of the potential energy, and it is given by:

$$\begin{aligned} \mathbf{f}(\mathbf{n}) &= -\sum_{k=1}^{12} \partial_{\mathbf{n}} V_k(\|\mathbf{m}_k\|) \\ &= -\sum_{k=1}^{12} \sigma_k(\|\mathbf{m}_k\|)(\mathbf{d}_k \otimes \mathbf{m}_k) \in \mathbb{R}^{18} \end{aligned} \tag{5}$$

where the scalars $\sigma_k = V_k'(\|\mathbf{m}_k\|)/\|\mathbf{m}_k\|$ are known as force densities with $V_k'(\|\mathbf{m}_k\|) = dV_k'(\|\mathbf{m}_k\|)/d\|\mathbf{m}_k\|$, and $\otimes$ denotes the Kronecker Product. Note that, because $\mathbf{d}_k \otimes \mathbf{m}_k = vec(\mathbf{m}_k \mathbf{d}_k^T)$ and $\mathbf{f}(\mathbf{n}) = vec(\mathbf{F}(\mathbf{n}))$, the force matrix $\mathbf{F}(\mathbf{n})$ is derived as:

$$\mathbf{F}(\mathbf{n}) = -\sum_{k=1}^{12} \mathbf{F}_k(\mathbf{n}) = -\sum_{k=1}^{12} \sigma_k(\|\mathbf{m}_k\|)\mathbf{m}_k \mathbf{d}_k^T \in \mathbb{R}^{3\text{x}6} \tag{6}$$

Let us define the diagonal matrix of force densities as

$$\Sigma(\mathbf{m}) = diag[\sigma_1(\|\mathbf{m}_1\|), \sigma_2(\|\mathbf{m}_2\|), \ldots, \sigma_{12}(\|\mathbf{m}_{12}\|)], \tag{7}$$

the force matrix can be rewritten with respect to member and connectivity matrices as follows:

$$\mathbf{F}(\mathbf{n}) = \mathbf{M}\Sigma(\mathbf{m})\mathbf{C} \tag{8}$$

Actually, force densities related with bars always satisfy the inequality $\sigma_b \leq 0$ and those with strings the inequality $\sigma_s \geq 0$, respectively, denoting that strings only carry tension and bars only carry compression. In addition, the structure will be in equilibrium if equation (8) is equal to zero.

Movements of the structure without any external force can be found using the stiffness matrix. The stiffness matrix $\mathbf{K}$ can be computed from derivative of equation (5) as follows:

$$\mathbf{K}(\mathbf{n}) = -\partial_{\mathbf{n}} \mathbf{f}(\mathbf{n}) \tag{9}$$

Skelton and Oliveira derived the stiffness matrix with respect to the connectivity matrix [32]. The stiffness matrix can expressed by a matrix form with the Kronecker product

$$\mathbf{K}(\mathbf{n}) = (\mathbf{C}^T \otimes \mathbf{I}_3) diag[\mathbf{L}_1(\mathbf{m}_1), \ldots, \mathbf{L}_{12}(\mathbf{m}_{12})](\mathbf{C} \otimes \mathbf{I}_3) \tag{10}$$

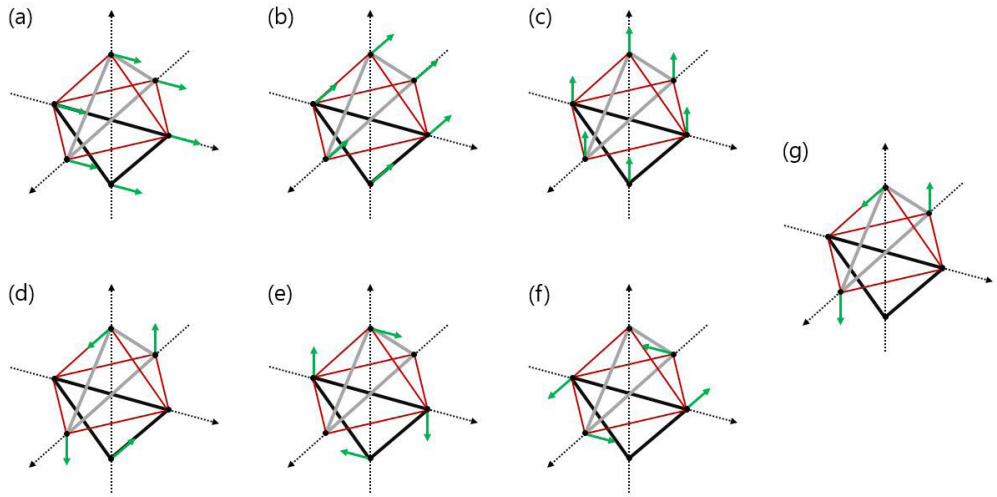

FIGURE 5. Seven rigid modal vectors, where rigid translation on (a) *Y*-axis, (b) *X*-axis, (c) *Z*-axis, rigid rotation around (d) *Y*-axis, (e) *X*-axis, (f) *Z*-axis, and (g) hinge joint rotation around *Y*-axis.

where

$$\mathbf{L}_k(\mathbf{m}_k) = \sigma_k(\|\mathbf{m}_k\|)\left[\mathbf{I}_3 - \frac{\mathbf{m}_k\mathbf{m}_k^T}{\|\mathbf{m}_k\|^2}\right] + V_k''(\|\mathbf{m}_k\|)\frac{\mathbf{m}_k\mathbf{m}_k^T}{\|\mathbf{m}_k\|^2} \tag{11}$$

Let us denote the eigenvalue and its corresponding eigenvector of the stiffness matrix K by ξ and $\mathbf{h}_\xi$, respectively. The eigenvalues and eigenvectors of the stiffness matrix are called modes and modal vectors, respectively, and thereby, they satisfy the following relationship:

$$\mathbf{K}\mathbf{h}_\xi = \xi\mathbf{h}_\xi, \quad \forall\mathbf{h}_\xi \neq 0 \tag{12}$$

Around an equilibrium point $\mathbf{n}$, the potential function can be approximated by second-order Taylor expansion. For small variation ϵ, the potential function can be expressed by:

$$V(\mathbf{n} + \epsilon\mathbf{h}) \approx V(\mathbf{n}) + \frac{1}{2}\epsilon^2\mathbf{h}^T\mathbf{K}\mathbf{h} \tag{13}$$

Changing nodes in the direction $\mathbf{h}$ leads to change of potential energy because the members in the structure yield internal forces. Also, the inertial force is derived from derivative of equation (13) as follows:

$$\mathbf{f}(\epsilon\mathbf{h}) = -\partial_{\mathbf{h}}V(\mathbf{n} + \epsilon\mathbf{h}) \approx -\epsilon\mathbf{K}\mathbf{h} \tag{14}$$

Form equations (12) and (14), there is no inertial force, namely, $\mathbf{K}\mathbf{h} = 0$ only when the eigenvalue of the stiffness matrix $\mathbf{K}$ is zero. This means all the members do not defrom in the direction $\mathbf{h}_\xi$, and thus, keeps the potential functon constant. Interestingly, at least six eigenvalues of $\mathbf{K}$ will always be zeros, and these eigenvalues are called rigid body modes.

Figure 5 shows rigid modal vectors of the proposed ligamentous structure. The ligamentous joint structure has seven zero modes. Figure 5(a)–(c) indicate rigid translations on Y, X, and Z-axis, respectively. Similarly Figure 5(d)–(f), respectively, depict rigid rotations around Y, X, and Z-axis.

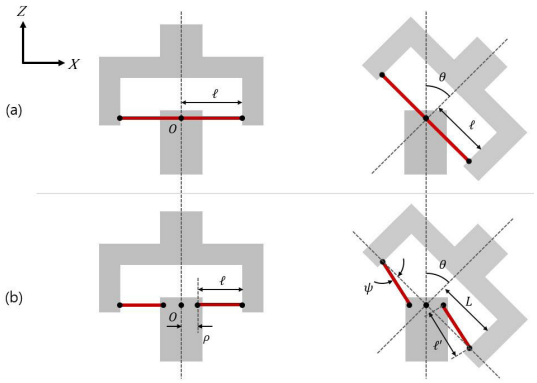

FIGURE 6. Cross-sectional view (a) basic structure (b) modified structure: in basic structure, string length is alwasy constant regardless of joint rotation. However, joint rotation brings a variation of string length in case of the modified structure, and this phenomenon generates force of restitution.

As mentioned above, Figure 5(a)–(f) account for the rigid body modes, which exist in common with every tensegrity structure. This means entire structure translates and rotates without change of its shape. Figure 5(g) ensures fearture of hinge joint in the proposed structure as it implies the following link composed of the nodes $\mathbf{n}_1$, $\mathbf{n}_3$, and $\mathbf{n}_5$ rotates around Y-axis.

IV. COMPLIANT FINGER DESIGN

A. FINGER MECHANISM WITH MODIFIED JOINT STRUCTURE

One of the advantages of ligamentous structure is, without any conformational change, to be able to bring spring effects to the joint. Figure 6 schematically shows the cross-sectional view of the joint in XZ plane. In the case of basic ligamentous structure introduced in above subsections, since the ends of two stings are joined at the same point, all strings maintain

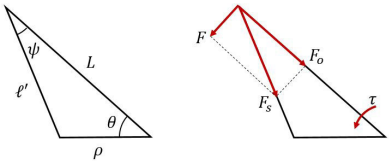

FIGURE 7. Triangle formed by joint rotation and its force contribution, where the triangle has three sides with their lengths ρ, L, and ℓ'. The tensile force in the string could be divided into the transversal force F_o to be canceled out to opposite side and the perpendicular force F to generate torque of restitution.

a constant length regardless of the amount of rotation of the following link. That is to say, the tensile forces of the strings do not change during the joint rotation. As a result, the following link is able to rotate freely. In practice, force of restitution is required to reduce the number of actuators only if the antagonistic actuations are not utilized. In this case, elastic elements such as springs and elastic strings could be embedded in the joint in traditional mechanisms. The ligamentous structure, however, is able to make the force of restitution by shifting the fixed position of the ends of strings as shown in Figure 6(b). The modified ligamentous structure brings length changes correlated with tensile forces in consequence of joint rotation.

Let us denote the length of string in the rest configuration by ℓ, the elongated length of string by ℓ' as a function of the joint rotation θ, the distance from the origin(center of rotation) to fixed position of the string by ρ, and the distance from the origin to another fixed position of the string by L, respectively. Then a triangle is constructed, which has three sides denoted by ℓ', L, and ρ as illustrated in Figure 7. The length of the string in the rotated configuration is expressed as a function of rotational angle θ as follows:

$$\ell' = \sqrt{L^2 + \rho^2 - 2L\rho\cos\theta}. \tag{15}$$

Since the change of string length is obtained as $\Delta\ell = \ell' - \ell$ with $\ell = L - \rho$ from the left side of Figure 6(b), we have

$$\Delta\ell = \ell' - L + \rho, \tag{16}$$

where the change in string length is always non-negative for $-\pi < \theta < \pi$. Above equation (16) becomes zero, $\Delta\ell = 0$, if and only if the joint does not rotate, $\theta = 0$, and it denotes the rest configuration because the minimal elastic energy is assured at the configuration.

In addition, the change in tensile force of the string is expressed with elastic coefficient k_s as follows:

$$F_s = k_s\Delta\ell. \tag{17}$$

Also, from formula about the area of triangle we know below relation:

$$\sin\psi = \frac{\rho}{\ell'}\sin\theta. \tag{18}$$

As depicted in the right side of Figure 7, the change in tensile force can be decomposed into the transversal force F_o related with joint translation and the perpendicular force F related with joint rotation. From the relationship between the perpendicular force and the tensile force, we know $F = F_s\sin\psi$. And using equation (18), the torque of restitution denoted by τ toward the rest configuration is obtained as follows:

$$\tau = FL = \frac{F_sL\rho}{\ell'}\sin\theta \tag{19}$$

Since the transversal force F_o passes through the center of rotation, it does not make any rotational torque but make translation force. However, another transversal force in opposite side, which has the same magnitue with opposite direction, is canceled out. On the other hand, since the perpendicular force F of the string in opposite side has the same magnitude and the same direction, and thus, the total torque of restitution of the joint becomes two times of equation (19). Interestingly, in the equation (19), we can know that the torque of restitution is directly proportional to the elastic coefficient k_s and the distance ρ from the center of rotation to the string origin.

The proposed finger is made up of four phalanges and three joints in common with other finger mechanisms. As the joints are based on the concept of tensegrity structure mentioned in previous section, there are not any contacts between phalanges during the movements, therefore there is no friction in the proposed finger mechanism. In addition, each joint is simultaneously capable of flexion by active tendon drive because the finger is a type of underactuated mechanism. On the other hand, extension in all the joints and adduction/abduction in MCP joint are passively operated by external force.

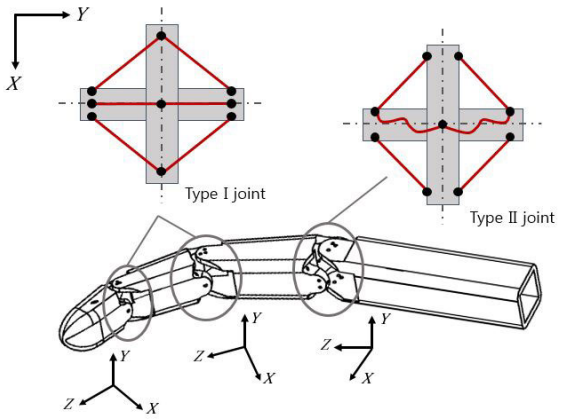

FIGURE 8. Perspective view of the proposed finger. For the passive extension of PIP and DIP joints, the modified structures are applied only to the direction of Y-axis. Whereas, the modified structure is applied to the both directions of X and Y-axis differently from IP Joints, for the passive abduction/adduction as well as the passive extension.

Figure 8 shows the proposed finger design with ligamentous joints. In PIP and DIP joints, the type I hinge joints proposed in previous section are installed, and the type II hinge joint is inserted in MCP joint of the finger. Also, the modified structure is applied to all the joints. For the passive extension of PIP and DIP joints, the modified structures

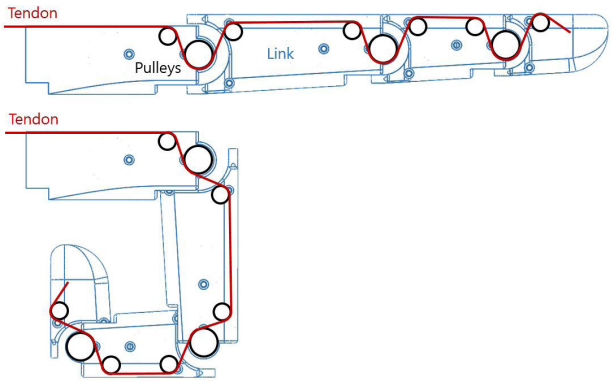

FIGURE 9. Tendon routing diaram for full extension and full flexion of the finger. Red line depicts the tendon path and black circle the pulleys to guide tendon. The finger includes three primary pulleys and six secondary pulleys for tendon drive. In the full extension and flexion, excessive movements of the joints are restricted by mechanical limits.

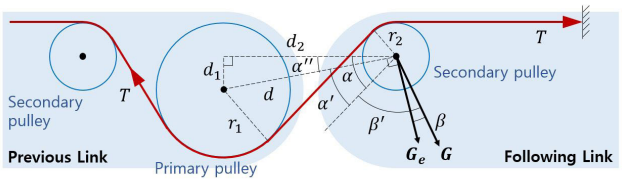

FIGURE 10. Schematic diagram of tendon routing, where each joint has one primary pulley and two secondary pulleys. For the simplicity, we assume that the tendon has an isotropic tensile strength T and the frictions of tendon are ignored.

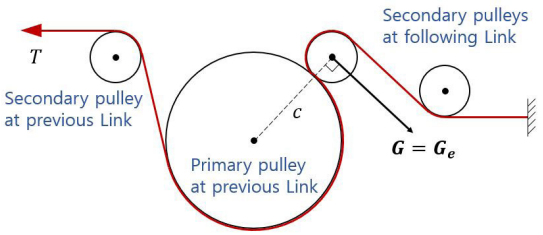

FIGURE 11. Optimized pulley positioning for tendon routing by Cabas *et al.* [33]. One primary pulley and three secondary pulleys were utilized for making actual force G equal to effective force G_e.

are applied only to the directions of Z axis. Different from the PIP and DIP joints, the modified structures are applied to the both directions of Y and Z axes in the case of MCP joint to implement passive extension, abduction and adduction. The range of motion between abduction and adduction is completely dependent on how much loose the substrings are at rest configuration becasue the tauten substrings restrict to move further.

B. TENDON ROUTING AND PULLEY LOCATION

Referring to the anatomy of human finger, there are two types of extrinsic muscles—flexors and extensors. These muscles contribute to flexion and extension of the finger joints, respectively. The ligamentous structure for rest configuration suggested in previous subsection has the force of restitution itself, and the joint returns to rest position naturally. Therefore, the finger installed ligamentous joint structures do not require particular parts to play a role as extensor. As a result, the proposed finger design only needs the driving tendon acting as an active flexor. Most of robotic fingers which only use flexor tendon include additional mechanical parts such as springs in order for the restoring force. Another feature of the proposed finger design is, without any additional parts, to enable to reduce the number of the driven tendons. In addition, depending on the locations where the ends of strings are fixed, the stiffness of the joint is able to be adjusted.

The design of tendon routing to be used in the proposed finger mechanism is illustrated in Figure 9. The finger has three primary pulleys and six secondary pulleys—each joint has one primary pulley and two secondary pulleys. For the sake of simplicity, let us make a few following assumptions: the tendon has isotropic tensile strength T; the frictions between pulley and tendon are ignored; the reaction force exerted on the previous links by the following link is sufficiently endured by ligamentous structure composed of strings. As shown in Figure 10, only the primary pulley inside the previous link and secondary pulley inside the following link will be treated for the mathematical modeling. Here, since the secondary pulley inside the previous link only guides the tendon to correct path, its radius and location do not affect the whole system. The center of primary pulley is located at the center of rotation of the joint. Let us suppose that G_e is an effective force to rotate the joint, G is actual force to rotate the joint come from tension of driven tendon, and d is a distance between the center of primary and secondary pulleys. From the force diagram shown in Figure 10, the following equations are obtained:

$$\begin{aligned} G &= 2T\cos\beta' \\ G_e &= G\cos\beta \end{aligned} \tag{20}$$

and other parameters are:

$$\begin{aligned} c &= \sqrt{{d_1}^2 + {d_2}^2} \\ \alpha' &= \sin^{-1}\frac{r_1 + r_2}{c} \\ \alpha'' &= \tan^{-1}\frac{d_1}{d_2} \\ \alpha &= \alpha' + \alpha'' \\ \beta' &= \frac{\pi - \alpha}{2} \\ \beta &= \alpha' + \beta' - \frac{\pi}{2} \end{aligned} \tag{21}$$

In tendon routing problem, one of the most important considerations is that the forces caused by tendon should be applied in the direction of rotation because the tangential force to the direction of rotation is corresponding to the loss. Cabas *et al.* had suggested the best solution that makes G_e to be maximum [33]. By making β' be zero, G can be turned into maximum. As a result, G_e becomes equal to G because β is to zero as well. However, one more pulley should be added for each joint to make β' be zero as shown in Figure 11. This method can generate the optimized force to rotate the joint

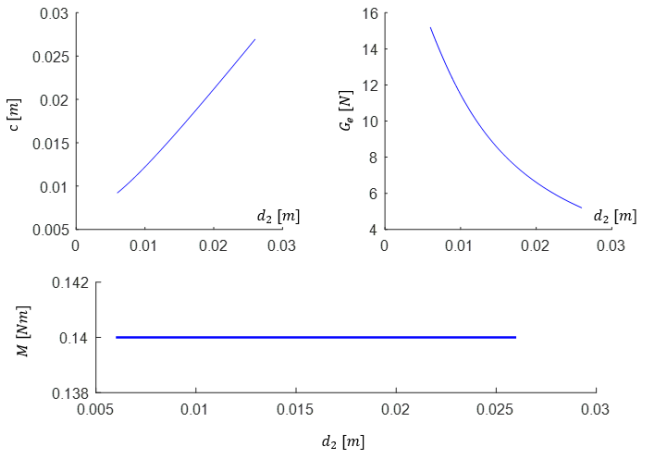

FIGURE 12. Variations of parameters according to the variation of the longitudinal distance d_2. According as d_2 increases, the moment arm c increases whereas the effective force to rotate the joint G_e decreases. The moment M, a multiplication of c and G_e, remains constant.

proportional to tensile force, by adding a secondary pulley one more. However, the more pulleys the finger have, not only the heavier whole weight of the finger is but also the higher friction occurs. For these reasons, this method is not applied to the proposed finger design which pursues lightweight and low friction. Instead, alternative solution is suggested in this subsection. Although G_e is not maximum, the solution does not require additional secondary pulley.

From the inverse trigonometric functions, the relationship between $\sin^{-1}$ and $\tan^{-1}$ is given by:

$$\sin^{-1}(x) = \tan^{-1}\left(\frac{x}{\sqrt{1-x^2}}\right)$$
$$\tan^{-1}(x) = \sin^{-1}\left(\frac{x}{\sqrt{1+x^2}}\right) \tag{22}$$

Combining equations (21) and (22), the condition for making β to zero is obtained:

$$d_1 = r_1 + r_2 \tag{23}$$

The force caused by tendon is applied only to the direction of rotation, only if above condition can be satisfied. Namely, without any additional pulleys, the actual force G becomes equal to the effective force G_e. Finally, the moment produced by the tension T can be obtained by multiplying the moment arm c as follows:

$$M = c \cdot G_e \tag{24}$$

Since pulleys have to be located inside phalanges, they cannot increase in radii infinitely. Moreover, it is physically impossible to make radii of pulleys smaller as well, because it would imply breaking tendon—actually the smaller the radius of secondary pulley is, the lager the effective force is. Once the radii of pulleys are determined to suit the finger size, only parameter d_2 remains undetermined.

Figure 12 shows variations of parameters according to the variation of the longitudinal distance d_2. According as d_2 increases, the moment arm c increases whereas the effective force to rotate the joint G_e decreases. Interestingly, the moment which is a multiplication of c and G_e nearly changes, namely, the parameter d_2 does not have any effect on the moment M. This means that the secondary pulley can be freely located on longitudinal direction in phalanges and that the moment to rotate the joint remains constant regardless of the location of pulley.

V. SIMULATIONS AND EXPERIMENTS

A. DESIGN PARAMETERS AND SIMULATIONS

Several properties of human finger have been known through the literatures. First of all, there are some linear ratios between MCP and PIP joint movements as well as MCP and DIP joint movements. Figliolini and Ceccarelli analyzed a natural closing motion of the finger by a sequence of snapshots captured using high-speed camera. As a result, they found that the rotation of each phalanx is not completely independent, but it has perticular linear ratios κ_1 between MCP and PIP joints and κ_2 between MCP and DIP joints as following form [34]:

$$\theta_P = \kappa_1 \theta_M,$$
$$\theta_D = \kappa_2 \theta_M. \tag{25}$$

Second, in all joints of the human finger, each range of motion is considered from 0° to 90°. Kapandji suggested the range of motion(ROM) of human finger joints from cadaveric study [35]. For an index finger, the ROM of the MCP joint is close to 90°, the ROM of the PIP joint a little bit exceeds 90°, but the ROM of the DIP joint is slightly less than 90°. For the sake of simplicity, the ROMs of all the joint angles are assumed as 0° to 90°. Also the length of each link was determined as suggested in Table 1.

For the tendon routing, four parameters such as r_1, r_2, d_1 and d_2 have to determined. The value of d_1 is to be a sum of r_1 and r_2 as suggested in the previous section. The value of d_2 has mostly no effect on the whole system, that is, r_1 and r_2 are only design parameters. For ease of implementation, r_1 and r_2 at all the joints are given as $4[mm]$ and $3[mm]$, respectively. It means that all joints in the finger have the same moments by the tendon T. For the joint design, the design parameters of each joint are ℓ, ρ and k_s. ℓ was determined to fit the size of each link as suggested in the Table 1, and k_s was set to be $10[N/mm]$ for all the joints. As mentioned above, each joint angle has two linear relationships denoted by equation (25), and we assume both proportional constants as $\kappa_1 = 0.75$ and $\kappa_2 = 0.5$, respectively. The values of ρ for each joint were suggested in the Table 1 for all the joints. Through the simulation study, we have obtained its results as shown in Figure 13 regarding the actual relationships between the MCP and IPs (PIP and DIP). Through Figure 14, an operation sequence can be understood, first, all the joints rotate simultaneously until the MCP joint arrives at 90°, second, both PIP and DIP joints rotate together until the PIP joint arrives at 90°. Finally, the DIP joint rotates to its end of the ROM.

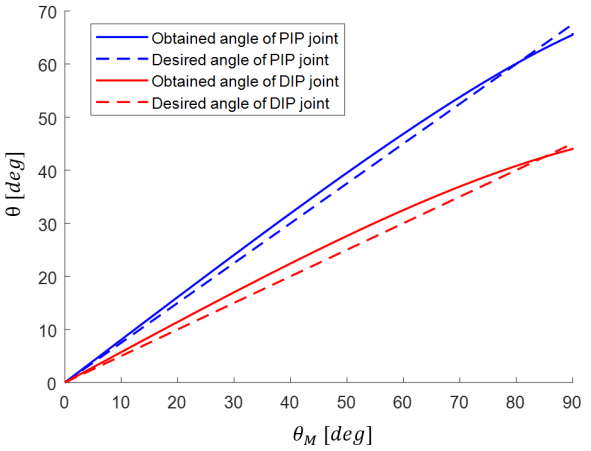

FIGURE 13. Angle variations of PIP and DIP joints with respect to angle of MCP joint from 0° to 90°. Dashed lines denote the angle variations corresponding to equation (25). Solid lines express actual angle variations of the proposed finger joints with the design parameters in Table 1.

TABLE 1. Design parameters for the joint suggested in Figures 6 and 7.

Joint	$\ell\ [mm]$	$\rho\ [mm]$	$k_s\ [N/mm]$
MCP	12	0.5	10
PIP	8	0.65	10
DIP	6.1	0.95	10

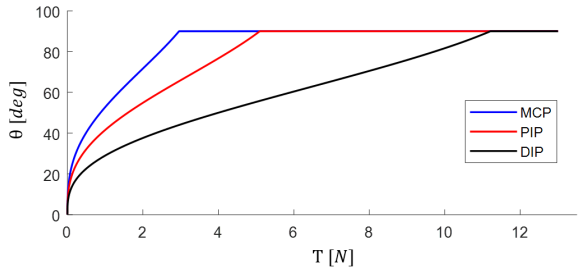

FIGURE 14. Angle variations of all the joints with respect to the variations in tensile force T. All the joints rotate simultaneously until the MCP joint arrives at the mechanical limit. And then the PIP and DIP joints rotate until the PIP joint arrives at the limit. The DIP joint is late to arrive at the limit.

Simulation regarding the finger flexion was also conducted. All the design parameters determined in the previous paragraph were used to flex fully all the joints of finger. The tensile force T needs a little over $10[N]$. During the simulation, it is increased from $0[N]$ to $10[N]$ by the increment of $0.1[N]$. Now we have the the simulation result shown in Figure 15. The figure graphically illustrates the sequence of grasping operations with the relationships between the joint angles and the applied tensile forces suggested in Figure 14. This finger was characterized by its fast reaction for small changes in tensile force when it starts to be actuated.

B. EXPERIMENTS WITH PROTOTYPE

For the performance test of the proposed finger mechanism, a prototype was manufactured based on the concepts introduced in the sections III and IV. The rigid bodies corresponding to phalanges of the robotic finger were 3D printed with ABS-like material. The fishing-lines made of fluorocarbon

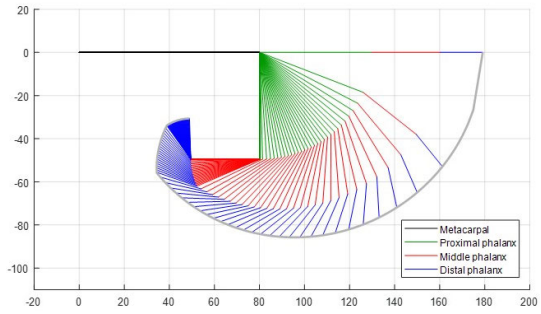

FIGURE 15. Simulation result in regard to finger flexion, where the tensile force driven by the tendon is increased from $0[N]$ to $10[N]$ with the increment of $0.1[N]$.

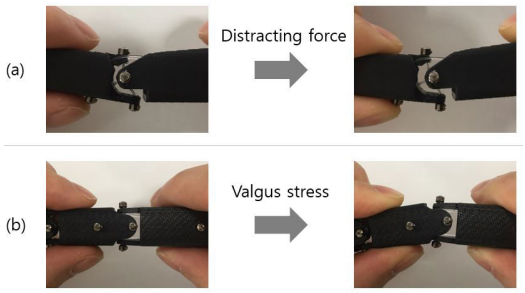

FIGURE 16. Compliance inherent in the proposed joint (a) against distracting force, (b) against valgus stress. Also, we can see that there is no contact between phalanges.

were used as the elastic strings and tendon drive. At present, the tendon for flexor was not controlled by actuator, but pulled by hand. In order to confirm characteristics of the proposed finger design, two cases were tested: the one was to test the compliant property of the joint structure against distracting/compressive forces and valgus/varus stresses; the other was to check the movements of the finger including active flexion, passive extension, and passive adduction/abduction.

Figure 16 shows the magnified pictures of the PIP joint of the prototype finger associated with distracting force and valgus stress, respectively. First, we can notice that the contact between two phalanges are not occurred because the weight of rigid bodies is sufficiently supported by tensile forces of the quadrangle strings and a pair of substrings, and hence, the joint maintains the equilibrium. Figure 16(a) shows the variation before and after applying distracting force to the joint. Compared two pictures, we can know that the gap between two phalanges is enlarged when the distracting force is applied, and a new force equilibrium is formed against the distracting force. Similarly, we can infer that the joint mechanism has compliance against the compressive force as well. Actually, the joint was more compliant against the compressive force than the distracting force because a pair of substrings slacken only when the compressive force is applied. As shown in Figure 16(b), the mechanism also had the compliance against valgus and varus stresses. Here, the stiffness is highly dependent on tensile forces of the substrings and relatively less dependent on those of quadrangle strings.

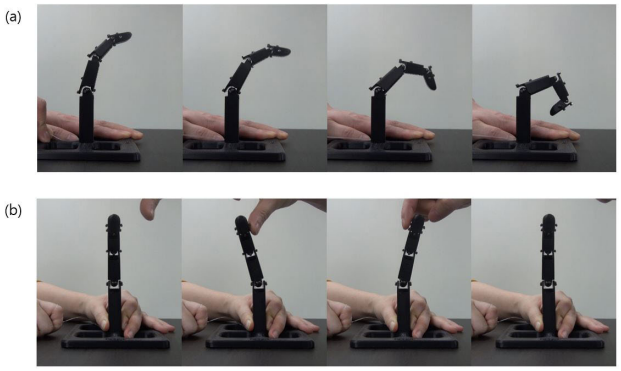

FIGURE 17. Movements of the proposed finger, where (a) the finger actively moves in flexion with underactuation, and (b) the finger passively moves in adduction and abduction. By tensile force of ligamentous joint structure, the finger returns to rest configuration without any exerted forces.

The proposed finger design actively moves only in flexion with underactuation, while the movements in extension and adduction/abduction are passively realized. Without the external forces, all joints automatically return to rest configuration by the restoring force in the quadrangle shaped strings and a pair of substrings. Successive snapshots of flexion motion of the finger are presented in Figure 17(a). We can see that each joint rotates simultaneously and proportionally with pulling the tendon. Also the extension is realized by the torque of restitution when the pulling force of driven tendon disappears. The ROM was mechanically limited by the contact between rigid body and mechanical limit stopper. In the human finger, active range of motion becomes different from passive range of motion. In other words, if the external force is applied when the human finger is actively in full flexion and extension, it moves more. This phenomena are called hyperflexion and hyperextension, respectively. Interestingly, the proposed finger design has these features along with the human finger. When excessive external force bigger than tensile force inherent in the joint is applied, the hyperextension and hyperflexion occur due to the capacity of compliance in the joint.

As shown in Figure 17(b), the finger performs adduction and abduction passively thanks to the modified structure suggested in the previous section. As previously stated, although PIP and DIP joints also have the capability of adduction/abduction by the inherent compliance, the tensile forces of the substrings in PIP and DIP joints were too much bigger than tensile force of restitution in MCP joint, and thus, the compliance in PIP and DIP joints nearly influenced on the adduction/abduction of MCP joint. The ROM between adduction and abduction is entirely dependent on how much loose the substrings are in rest configuration, because the taut substrings due to adduction and abduction severely restrict further movement by their tensile forces.

VI. CONCLUSION

This paper has presented the compliant finger design composed of two types of bio-inspired hinge joints. Each joint structure was inspired by ligamentous structure forming a synovial joint of the human. Quadrangular shaped four main strings and a pair of substrings have mimicked the articular capsule and the collateral ligaments, respectively. The functions of these strings were also much similar to those of ligaments in the synovial joints. Indeed the joint structure was based on tensegrity structure composed of elastic strings and rigid bodies. Thereby, the finger mechanism was inherited the features of tensegrity. In addition, the modified structure was introduced to yield the torque of restitution toward the rest configuration when the deriven-tendon force for joint flexion was disappeared. Consequently, the proposed finger mechanism has realized active flexion, passive extension, and passive abduction/addunction, as underatuated finger.

The mechanism has several benefits inherited from human ligamentous structure and tensegrity system. One of the great advantages is to have the compliance against external forces, which is obviously different from the traditional mechanical joint. As most mechanical joint uses metallic parts such as a bearing and harmonic drive, it is hard to be compliant against axial force. The proposed mechanism, however, is compliant to any forces from all the directions. In addition, the mechanism is lightweight and has no rigid body contact during movement, which are also the features of tensegrity system. Finally, the mechanism is free from the complicated tendon routing problem. The modified joint structure has achieved self-actiong joint extension, and efficient force to rotate the joint has been generated regardless of the longitudianl location of the secondary pulleys. On the other hand, the mechanism has some drawbacks. Since many strings are used, complex mathematical analysis is demanded. It also has the endemic problem how the strings are securely anchored in the rigid body as many wire-driven mechanisms have.

In the near future, we are planning to introduce a hand model that includes the finger proposed in this paper. In order to achieve this purpose, however, we have to resolve the following issues. First of all, for the constant tension of the strings, we have to work out a way to hold the strings firmly. This is a very important matter because accurate quantitative data can be obtained through experiments only when this problem is solved. After that, we have to conduct experiments more for obtaining quantitative data to show the effectiveness of the proposed mechanism and to be used for control of the finger. For instance, the relationship between driven-tendon and fingertip forces, the joint stiffness against external forces, the variation of center of rotation of the joint with respect to pay-load and so forth should be conducted. In addition, for the precise control of the proposed finger mechanism, its dynamics and kinematics should be derived and considered. For trade-off between compliance and stiffness of the joints, some criteria in choosing the stiffness of the strings and in determining the fixed positions of the strings should be also found in mathematical expressions.

REFERENCES

[1] S. Collins, A. Ruina, R. Tedrake, and M. Wisse, "Efficient bipedal robots based on passive-dynamic walkers," *Science*, vol. 307, no. 5712, pp. 1082–1085, Feb. 2005.

[2] J.-S. Koh, E. Yang, G.-P. Jung, S.-P. Jung, J. H. Son, S.-I. Lee, P. G. Jablonski, R. J. Wood, H.-Y. Kim, and K.-J. Cho, "Jumping on water: Surface tension-dominated jumping of water striders and robotic insects," *Science*, vol. 349, no. 6247, pp. 517–521, Jul. 2015.

[3] P. S. Sreetharan and R. J. Wood, "Passive aerodynamic drag balancing in a flapping-wing robotic insect," *J. Mech. Des.*, vol. 132, no. 5, 2010, Art. no. 051006.

[4] E. Garcia, J. C. Arevalo, G. Muñoz, and P. Gonzalez-de-Santos, "On the biomimetic design of agile-robot legs," *Sensors*, vol. 11, no. 12, pp. 11305–11334, Nov. 2011.

[5] L. Li, H. Godaba, H. Ren, and J. Zhu, "Bioinspired soft actuators for eyeball motions in humanoid robots," *IEEE/ASME Trans. Mechatronics*, vol. 24, no. 1, pp. 100–108, Feb. 2019.

[6] S. Shirafuji, S. Ikemoto, and K. Hosoda, "Development of a tendon-driven robotic finger for an anthropomorphic robotic hand," *Int. J. Robot. Res.*, vol. 33, no. 5, pp. 677–693, Apr. 2014.

[7] S. Ikemoto, F. Kannou, and K. Hosoda, "Humanlike shoulder complex for musculoskeletal robot arms," in *Proc. IEEE/RSJ Int. Conf. Intell. Robots Syst.*, Oct. 2012, pp. 4892–4897.

[8] A. Ananthanarayanan, M. Azadi, and S. Kim, "Towards a bio-inspired leg design for high-speed running," *Bioinspir. Biomim.*, vol. 7, no. 4, Dec. 2012, Art. no. 046005.

[9] Z. Xu and E. Todorov, "Design of a highly biomimetic anthropomorphic robotic hand towards artificial limb regeneration," in *Proc. IEEE Int. Conf. Robot. Autom. (ICRA)*, May 2016, pp. 3485–3492.

[10] A. D. Deshpande, Z. Xu, M. J. V. Weghe, B. H. Brown, J. Ko, L. Y. Chang, D. D. Wilkinson, S. M. Bidic, and Y. Matsuoka, "Mechanisms of the anatomically correct testbed hand," *IEEE/ASME Trans. Mechatronics*, vol. 18, no. 1, pp. 238–250, Feb. 2013.

[11] S. W. O'Driscoll, "Elbow instability," *Acta Orthopaedica Belgica*, vol. 65, no. 4, pp. 404–415, 1999.

[12] H. Gurbuz, T. Kutoglut, and R. Mesut, "Anatomical dimensions of anterior bundle of ulnar collateral ligament and its role in elbow stability," *Folia Medica*, vol. 47, no. 1, pp. 47–52, 2005.

[13] Y. Minamikawa, E. Horii, P. Amadio, W. Cooney, R. Linscheid, and K.-N. An, "Stability and constraint of the proximal interphalangeal joint," *J. Hand Surg.*, vol. 18, no. 2, pp. 198–204, Mar. 1993.

[14] T. R. Kiefhaber, P. J. Stern, and E. S. Grood, "Lateral stability of the proximal interphalangeal joint," *J. Hand Surg.*, vol. 11, no. 5, pp. 661–669, Sep. 1986.

[15] R. N. Hotchkiss and A. J. Weiland, "Valgus stability of the elbow," *J. Orthop. Res.*, vol. 5, no. 3, pp. 372–377, 1987.

[16] P. K. Levangie and C. C. Norkin, *Joint Structure and Function: A Comprehensive Analysis*, F. A. Davis, Ed. Philadelphia, PA, USA: Davis, 2011.

[17] H. Son, G. Lee, C. Lee, and Y. Choi, "Underactuated tendon-driven finger design with bio-inspired ligamentous joint mechanism," in *Proc. IEEE Int. Conf. Cyborg Bionic Syst. (CBS)*, Oct. 2018, pp. 171–176.

[18] P. L. Ephraim, S. T. Wegener, E. J. MacKenzie, T. R. Dillingham, and L. E. Pezzin, "Phantom pain, residual limb pain, and back pain in amputees: Results of a national survey," *Arch. Phys. Med. Rehabil.*, vol. 86, no. 10, pp. 1910–1919, 2005.

[19] N. Kashiri, M. Laffranchi, D. G. Caldwell, and N. G. Tsagarakis, "Dynamics and control of an anthropomorphic compliant arm equipped with friction clutches," *IEEE/ASME Trans. Mechatronics*, vol. 21, no. 2, pp. 694–707, Apr. 2016.

[20] S. Wolf and G. Hirzinger, "A new variable stiffness design: Matching requirements of the next robot generation," in *Proc. IEEE Int. Conf. Robot. Autom.*, May 2008, pp. 1741–1746.

[21] S. Yoon, S. Kang, S. Kim, Y. Kim, M. Kim, and C. Lee, "Safe arm with MR-based passive compliant joints and visco-elastic covering for service robot applications," in *Proc. IEEE/RSJ Int. Conf. Intell. Robots Syst.*, Oct. 2003, pp. 2191–2196.

[22] M. Cestari, D. Sanz-Merodio, J. C. Arevalo, and E. Garcia, "An adjustable compliant joint for lower-limb exoskeletons," *IEEE/ASME Trans. Mechatronics*, vol. 20, no. 2, pp. 889–898, Apr. 2015.

[23] R. Deimel and O. Brock, "A compliant hand based on a novel pneumatic actuator," in *Proc. IEEE Int. Conf. Robot. Autom.*, May 2013, pp. 2047–2053.

[24] N. Tan, X. Gu, and H. Ren, "Simultaneous robot-world, sensor-tip, and kinematics calibration of an underactuated robotic hand with soft fingers," *IEEE Access*, vol. 6, pp. 22705–22715, 2018.

[25] L. U. Odhner, L. P. Jentoft, M. R. Claffee, N. Corson, Y. Tenzer, R. R. Ma, M. Buehler, R. Kohout, R. D. Howe, and A. M. Dollar, "A compliant, underactuated hand for robust manipulation," *Int. J. Robot. Res.*, vol. 33, no. 5, pp. 736–752, Apr. 2014.

[26] R. E. Skelton, R. Adhikari, J. Pinaud, and W. Chan, "An introduction to the mechanics of tensegrity structures," in *Proc. IEEE Conf. Decis. Control*, Dec. 2001, pp. 4254–4259.

[27] G. Scarr, "A consideration of the elbow as a tensegrity structure," *Int. J. Osteopathic Med.*, vol. 15, no. 2, pp. 53–65, Jun. 2012.

[28] R. E. Skelton and M. C. de Oliveira, *Tensegrity Systems*. New York, NY, USA: Springer, 2009.

[29] M. Arsenault and C. M. Gosselin, "Kinematic, static, and dynamic analysis of a spatial three-degree-of-freedom tensegrity mechanism," *J. Mech. Des.*, vol. 128, no. 5, pp. 1061–1069, Sep. 2006.

[30] L. Birglen, T. Lalibert, and C. M. Gosselin, *Underactuated Robotic Hands*. Berlin, Germany: Springer, 2007.

[31] A. Minami, K.-N. An, W. P. Cooney, R. L. Linscheid, and E. Y. S. Chao, "Ligamentous structures of the metacarpophalangeal joint: A quantitative anatomic study," *J. Orthop. Res.*, vol. 1, no. 4, pp. 361–368, 1983.

[32] R. E. Skelton and M. C. Oliveira, *Tensegrity Systems*. New York, NY, USA: Springer, 2009.

[33] R. Cabas, L. Cabas, and C. Balaguer, "Optimized design of the underactuated robotic hand," in *Proc. IEEE Int. Conf. Robot. Autom. (ICRA)*, Jul. 2006, pp. 982–987.

[34] G. Figliolini and M. Ceccarelli, "A novel articulated mechanism mimicking the motion of index fingers," *Robotica*, vol. 20, no. 1, pp. 13–22, Jan. 2002.

[35] A. I. Kapandji, *The Physiology of the Joints*, vol. 1. London, U.K.: Churchill Livingstone, 2007.

GEON LEE received the B.S. degree from the Department of Electrical and Electronic Computer Engineering, Hanyang University, South Korea, in 2008, and the M.S. degree in electrical, electronic, control and measurement engineering from Hanyang University, in 2010, where he is currently pursuing the Ph.D. degree with the Department of Electronic System Engineering. He was a Research Scientist with the Interaction and Robotics Research Center, Korea Institute of Science and Technology (KIST), from 2011 to 2013, and the Research Institute of Engineering and Technology, Hanyang University, from 2013 to 2015. His current research interests include bioinspired structures, mechanisms of robotic hand and arm, and tendon drive.

YOUNGJIN CHOI (Senior Member, IEEE) was born in Seoul, South Korea, in 1970. He received the B.S. degree in precision mechanical engineering from Hanyang University, Seoul, in 1994, and the M.S. and Ph.D. degrees in mechanical engineering from POSTECH, Pohang, South Korea, in 1996 and 2002, respectively. Since 2005, he has been a Professor with the Department of Electrical and Electronic Engineering, Hanyang University, Ansan, South Korea. From 2002 to 2005, he was a Senior Research Scientist with the Intelligent Robotics Research Center, Korea Institute of Science and Technology (KIST). From 2011 to 2012, he was a Visiting Researcher with the University of Central Florida, USA. His research interests include biorobotics and control theory. He was an Associate Editor of the IEEE TRANSACTIONS ON ROBOTICS, from 2010 to 2014, and the IEEE ROBOTICS AND AUTOMATION LETTERS, from 2016 to 2018. Since 2018, he has been a Senior Editor of the IEEE ROBOTICS AND AUTOMATION LETTERS.